Indian Journal of Experimental Biology
Vol. 60, September 2022, pp. 727-733
DOI: 10.56042/ijeb.v60i09.41848

HPLC/QTOF-MS metabolomics analysis applied to identify skin biomarkers of UVC-induced skin injury in mice and preventive effects of abietic acid

Nianyun Yang[1]*, Jiaojiao Qian[1] & Lijuan Tian[2]

[1]Jiangsu Plant Medicine Research and Development Center, Nanjing University of Chinese Medicine, Nanjing 210023, China
[2]Technique Institute, Jinling Pharmaceutical Co. Ltd., Nanjing 210009, China

Received 16 October 2020; *revised 09 September 2021*

Abietic acid (AA) is a main constituent from pine resin, which has definite therapeutical effects for treating skin ulcers and tumor. Here, we explored the metabolome changes in skin tissues of mice with UVC-induced skin injury treated with AA by a HPLC-QTOF-MS/MS method. Model mice were induced with UVC irradiation. Skin histopathological changes were examined by routine HE staining. Metabolomic analysis technology and pattern recognition statistical method were applied to analyze the metabolites in the skin tissues of mice to study the therapeutic effect of AA on UVC-induced skin injury in mice. Ceramides, sphingosines, glycyl-L-glutamine, *dihydroorotic acid*, adenosine, dCMP and lyso-phosphatidylcholines can be used as biomarkers of UVC-induced skin injury. AA can improve the pathological tissue from the pathway of skin lipid and purine pyrimidine metabolism to achieve the therapeutic effect. AA can effectively treat UVC-induced skin injury in mice.

Keywords: Adenosine, Ceramides, dCMP, Pine resin, *Pinus massoniana*

Pine resin is a solid resin retained after the removal of volatile oil from *Pinus massoniana* or other plants of the same genus. Pine resin could treat carbuncle and malignant skin ulcer as a traditional Chinese medicine[1]. Pine resin contains mixtures of several related diterpene acids, primarily abietic acid (AA) and dehydroabietic acid, which have definite therapeutical effects for treating skin ulcers and tumor[2]. AA and dehydroabietic acid have strong inhibitory effect on rat breast cancer induced by dimethylbenzoanthracene (DMBA), papilloma activated by phorbol ester and human carcinoma cell lines A431 *in vitro*[3]. Pine resin and AA had therapeutic effects on skin cancer of mice, the possible mechanisms of which might be decreasing the expression of cytokeratins (CK10 and CK5/6) and matrix metalloproteinases (MMP-1 and MMP-3)[4,5]. AA could reduce the metastasis of murin melanoma cells, thereby constituting an adjuvant treatment for metastasis control[6]. AA could act as a PPAR α/γ dual activator to inhibit UVB-induced MMP-1 expression and age-related inflammation by suppressing NF-κB and the MAPK/AP-1 pathway and can be a useful agent for improving skin photoageing[7].

*Correspondence:
E-Mail: nianyunyang@hotmail.com

UV radiation induces acute and chronic reactions in human and animal skin. Chronic repeated exposures are the primary cause of benign and malignant skin tumors. UV-induced skin injury in mice presents similar process of human skin photo damage. The biological effects and mechanism of UV-induced skin injury is mostly focused on physiological and biochemical index and macro-molecular markers[8].

According to the wavelength, ultraviolet (UV) can be divided into UVA, UVB and UVC. UVA has strong skin tissue penetration, while UVC can induce more irradiation damage on epiderm at the same dose[9]. When exposed to ultraviolet light, many enzymes and proteins are activated or inhibited to produce a large amount of oxygen free radicals[10]. These changes affect skin barrier function and cuticle structure significantly[11]. UVA and UVB irradiation could cause abnormal structure of stratum corneum lipids and reduce ceramide content, which lead to damage of skin barrier function[12]. Research on small molecule only aimed at local variations. However, systematic and comprehensive evaluation on endogenous small molecular markers changes caused by UVC and AA intervention has seldom been reported.

Metabolomics refers to the qualitative and quantitative analysis of all metabolic components in

specific biological samples. Metabolomics focused on the endogenous compounds of small molecules in body fluids and tissues. Metabolomics has more advantages than genomics and proteomics in discovering active substances, revealing metabolism rules and *in vivo* drug analysis[13]. In this study, we investigated the effects of AA on UVC-induced skin injury in mice, specifically the pathological changes and metabolomics of epithelial tissue.

Materials and Methods

Animals

The forty 6-week-old male SPF BALB/c mice (21-25 g) were obtained from Jiangning District, Nanjing Qinglongshan Animal Center (Certificate number No.201812610). The animals were housed in groups of 10 (details given below) under environmentally controlled conditions with free access to water and standard food. Food was withheld overnight prior to experiments while water was still provided ad libitum. The handling and use of animals were in accordance to the institutional guidelines.

Drugs and reagents

5-Fluorouracil (No.NO2N8W47246) was from Shanghai Yuanye Biotechnology Co., Ltd. Abietic acid (No.20150506) was bought from Anhui Haizhou Haiguang TCM Yinpian Co., Ltd. Anhydrous Ethanol (No.100092683) and Xylene (No. 10023418) was from Sinopsin Group Chemical Reagent Co., Ltd. HE dye (No.G1005), differentiation liquid (No.g1005-3) and blue return liquid (No.g1005-4) were from Servicebio. Neutral gum (No.10004160) was from Sinopharmaceutical Chemical Reagent Co., Ltd.

Animal experimental design

The animals were randomly divided into 4 groups of 10 mice per group, and all groups were given free diet. The mice were denuded by depilatory cream prior to shaving for a rectangle area of 3×5 cm on every animal's back. Gr. I served as a normal control. UVC-induced skin injury was induced in groups II-IV by the application of UVC. Mice were irradiated by UVC (56 mJ/cm^2) 30 min every day. Gr. III received 0.1 mL AA solution topically once a week (4 mg·mL^{-1}). Gr. IV was given 0.1 mL 5-FU acetone solution (2.0 mg· mL^{-1}) topically on the dorsal skin area after hair removed once a week, which served as a positive control. The experiment lasted for eight weeks. At the end of experiment, some local back skin tissues were collected and fixed in 10% formalin solution for histological examination. About 0.4 g pathological skin tissues were freshly collected, rinsed with phosphate buffer solution and wiped by filter paper. The tissues were accurately weighed immediately, and cutted into pieces. The pieces were added into the precooled EP tubes with 1.5 mL 60% methanol solution, and stored at −80℃ for further metabolomics analysis.

Histological analysis of skin tissue

After formalin fixation for 36 h, the back skin samples were sectioned and stained with haematoxylin-eosin (H&E) and subsequently examined under a light microscope (Nikon Eclipse E100, Japan) for general histopathology examination. The extent of skin damage was evaluated on H&E slides. The histological changes were observed and scored.

HPLC-*Q*-TOF-MS/MS analysis

The skin tissue samples were defrosted, which were quickly homogenized in ice-water bath. After centrifugation the supernatant was filtrated with 2.5 μm micromembrane. About 10 μL filtration of each sample was injected into chromatography. The chromatographic conditions are as follows: Eclipse Plus C18 column (2.1 mm×150 mm, 1.8 μm); The flow rate of mobile phase was 0.5 m L/min using 0.1% formic acid aqueous solution (A) and 0.1% formic acid acetonitrile (B). The injection volume was 10 μL, and the running time was 50 min after gradient elution, starting at 5% B, increasing to 30% within 15 min, 60% within 25 min, and 95% within 50 min. Automatic sampler control temperature is 5℃; and the column temperature was adjusted to 35℃. The main parameters of mass spectrometry were as follows: a positive ion mode of electrospray ion source (ESI) was selected; Collection range: m/z 50-1000; N2 was used as dry gas, the dry gas flow rate was 10L/min, and the temperature was set at 350℃. The positive ion capillary voltage was 4000V, and the fragmentation voltage was 160V. Atomized gas pressure was 35 psi. The collection rate was 2 spectrums, and the data were stored in Centroid mode. In the process of data collection, m/z 922.0098 and 121.0509 are used as reference ions in the positive ion mode to test the operation stability of the instrument in this mode and calibrate the real-time quality deviation of the instrument. The proposed method is validated based on detection of quality control (QC) sample, which is mixed by each 100 μL of test sample. First QC sample was run through HPLC 5 times to balance the system. QC sample was repeatedly run at

intervals of 5 experimental samples detection to measure the stability of the analysis system.

Peak identification and data analysis

Peakview™ 1.7 software was applied to analyze the total ion current under positive ion mode; Markerview ™ 2.0 was applied to match and normalize mass spectra peaks. The main parameters were set as follows. Mass error was 0.1; background noise elimination level was 10.0; initial and final retention time was 0 and 50 min respectively; the molecular weight distribution was in the range of 90 to 1000 Da. The peaks were identified by molecular or quasi-molecular ions and fragment ions according to references. The peak area data were imported into simca-p (V11.5) software, and differences in metabolic profiles among groups were distinguished by principal component analysis (PCA) model. Potential metabolite markers were screened according to the variable importance in projection (VIP) by partial least squares discriminant analysis (PLS-DA) model, and the metabolic pathways were analyzed by KEGG database (https://www.kegg.jp/).

This study was approved by the Ethics Review Committees of Nanjing University of Chinese Medicine of China.

Results

Histopathological examination

At the end of experiment, the back skin of mice in Gr. I was intact, elastic and pink, and showed no epidermal hyperplasia. The back skin of mice in Gr. II showed epidermal hyperplasia, and exogenous small sarcomas could be found in a small number of mice. The skin of mice in Gr. III was intact and thickened. The skin of mice in Gr. IV was intact, and erythema appeared in a few mice.

The microscopic changes were equally significant. In the normal control Gr. I, staining slices showed no significant abnormality. The dermal cells are normal in shape and closely arranged and have rich collagen. The structures of hair follicle and sebaceous gland were normal. In the UVC Gr. II, epidermis showed local mesh necrosis accompanied by infiltration of more pus cells. Necrotic epidermis also showed massive scab with inflammatory exudates and hypersecretory keratin. Partial epidermis became moderately thick and squamous cells proliferated. There were more inflammatory cells infiltrated in dermis. Structural destruction of sebaceous glands was occasionally observed. HE staining showed epidermal cells of Gr. II arranged in disorder and a few multinucleated giant cells. In AA administration Gr. III, partial epidermis became slightly thick and squamous cells weakly proliferated. There were a small amount of neutrophils and lymphocytes infiltrated in dermis. Hair follicles and sebaceous glands revealed no obvious abnormalities. In 5-FU administration Gr. IV, partial epidermis became slightly thick and squamous cells weakly proliferated. There were a small amount of lymphocytes infiltrated in dermis. No obvious abnormalities were observed in the dermal hair follicles and sebaceous glands. Compared with the models, the skin pathological changes of each medication group were significantly improved, which were represented in Fig. 1.

Skin metabolomics

HPLC-MS analysis and metabolite identification

The skin tissue samples of Groups I-III were analyzed by HPLC-QTOF-MS. The total ion chromatogram (TIC) is shown in the Fig. 2. The experimental results showed that the chromatograms of metabolites were obviously different in all samples, and the content is different in all samples. On the basis of the analysis with Peakview™, a total of 58 metabolites were quantified. Content changes in the metabolite profile were analyzed and 15 metabolites exhibited a difference (P <0.01) among three groups by ‘t’ test, as is shown in Table 1.

Differential metabolite discovery

Principal component analysis

It was difficult to detect differential metabolites directly from data on TIC. Therefore, it’s necessary to conduct pattern recognition of peak area of three

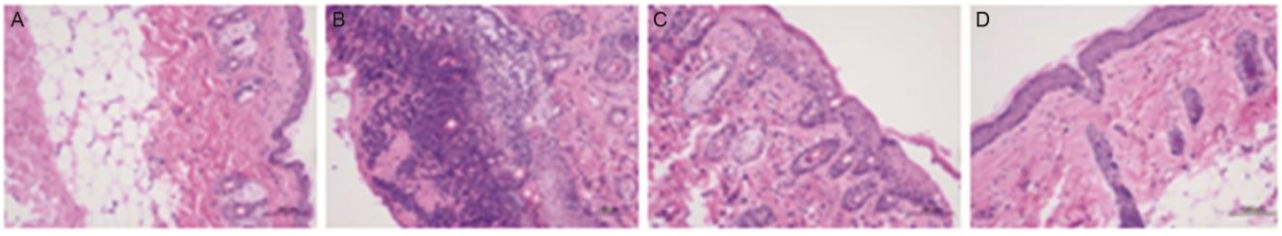

Fig. 1 — Epithelial pathomorphological changes of experimental skin cancer in mouse (200X)

groups. 24 common peaks were identified through the comparison of retention time and m/z, and the area data of each common peak was imported into SIMCA-p (V11.5) software. Principal component analysis (PCA) is a statistical procedure that uses an orthogonal transformation to convert a set of observations of possibly correlated variables into a set of values of linearly uncorrelated variables called principal components. PCA is a dimension reduction method and sensitive to the relative scaling of the original variables. The data of different groups were performed with PCA by model recognition and plotting the graph of their scores, and the different agents can be distinguished in the scattered plots.

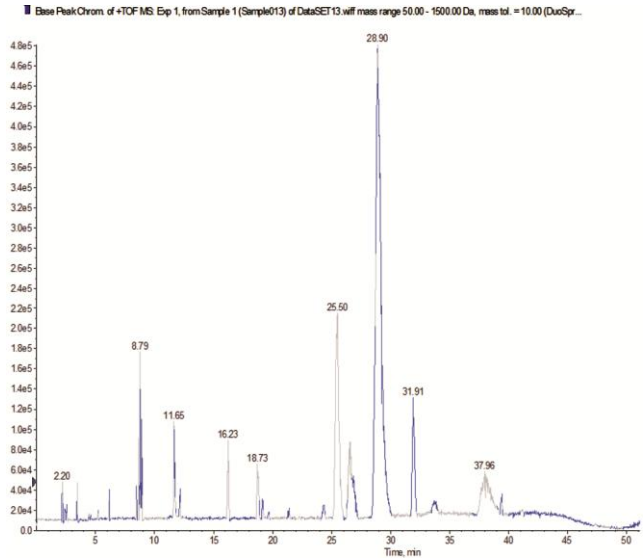

Fig. 2 — HPLC-QTOF total positive ion flow chromatogram in model group

Fig. 3 A(ii) is the factor loading diagram of PCA analysis between the normal control and model groups, which showed that P24, P23, P1 and P8 make a greater contribution to distinguish two Gr. I and II. Fig. 3 A(i) is the score chart of of PCA analysis between the normal control and model groups (Gr. II and III), which showed that the difference of metabolites existed significantly between different groups. Gr. II and III were clearly separated by vertical axis. Fig. 3 B(ii) is is the factor loading diagram of PCA analysis between the abeitic acid administered group and the model group, which showed that P21, P36 and P15 make a greater contribution to distinguish two Gr. II and III.

PCA analysis showed that there is a significant difference between the normal group and UVC-induced skin injury model group, indicating that UVC can successfully cause the skin damages. The difference between the model group and the AA treatment group was significant. Combining the results of pathomorphic analysis, it indicated that AA had obvious therapeutic effect on UVC-induced skin injury.

Partial least square discriminant analysis

Partial least square discriminant analysis (PLS-DA) is a multidependent variable regression modeling method. PLS-DA can better distinguish the differences between groups. Supervised pattern recognition analysis method can tend to extract the variable information that is conducive to sample classification. Therefore, in order to find differential metabolites among the three groups, the supervised partial least square analysis (PLS-DA) method was

Table 1 — VIP values and molecular information of different metabolites

Pike	M/Z positive	Molecular formula	Chemical name	Peak area I	Peak area II	Peak area III	VIP
22	526.4835	$C_{32}H_{63}NO_4$	Cer(t18:1/14:0)	2765296±227060*	45055±1999	1602285±100965*	1.0944±0.7020
25	568.5305	$C_{35}H_{69}NO_4$	Cer(t18:1/17:0)	20175402±231012*	673666±101453	1319700±190014*	1.0908±0.9151
14	188.0712	$C_{11}H_9NO_2$	Indoleacrylic acid	461516±490142*	134254±18745	429906±89014*	1.0907±0.6212
9	268.1032	$C_9H_{17}NO_8$	Adenosine	0*	517753±59104	0*	1.0899±0.5201
5	308.0648	$C_9H_{14}N_3O_7P$	dCMP	0*	174537±19249	0*	1.0898±0.9740
35	480.3090	$C_{23}H_{46}NO_7P$	LPC 15:1	0*	658747±100215	0*	1.0896±0.7431
33	454.2934	$C_{21}H_{44}NO_7P$	LPC 13:0	0*	331598±59954	0*	1.0895±0.4784
28	478.4624	$C_{28}H_{53}NO_4$	Cer(t18:1/10:1)	1012209±189124*	267788±49578	1001457±200148*	1.0850±0.9190
34	582.5421	$C_{36}H_{71}NO_4$	Cer(t18:1/18:0)	201243±19978*	110412±17410	187142±20147*	1.0810±0.4312
38	520.4730	$C_{33}H_{61}NO_3$	Cer(d18:1/15:1)	5651932±754561*	432151±59971	2021108±199456*	1.0662±0.2275
17	318.3008	$C_{18}H_{39}NO_3$	Phytosphingosine	1773452±299410*	704378±164121	929083±124151*	1.0479±0.7270
26	526.4835	$C_{32}H_{63}NO_4$	Cer(t16:1/16:0)	379995±39456*	45055±9410	223477±45011*	1.0335±0.5841
23	415.2121	$C_{24}H_{30}O_6$	Monobehenin	3104571±491240*	224516±39472	449332±49947*	1.0318±0.9874
27	502.4471	$C_{29}H_{59}NO_5$	Cer(t16:0/h11:0)	1442287±201423*	132340±19743	208340±21413*	1.0304±0.7591
36	415.2121	$C_{24}H3_0O_6$	Glyceryl eicosate acetate	343301±29945*	224942±30912	250328±40915*	1.0269±0.8810

[Cer(t18:1/14:0) is tetradecanoic amide, N-[2,5-dihydroxy-1-(hydroxymethyl)-3-heptadecenyl]-, and so on; * P <0.01 compared with Gr. II. Gr. I, normal control; Gr. II, experimental control; and Gr. III received 0.1 mLAA solutiontopically once a wk(4 mg mL^{-1})]

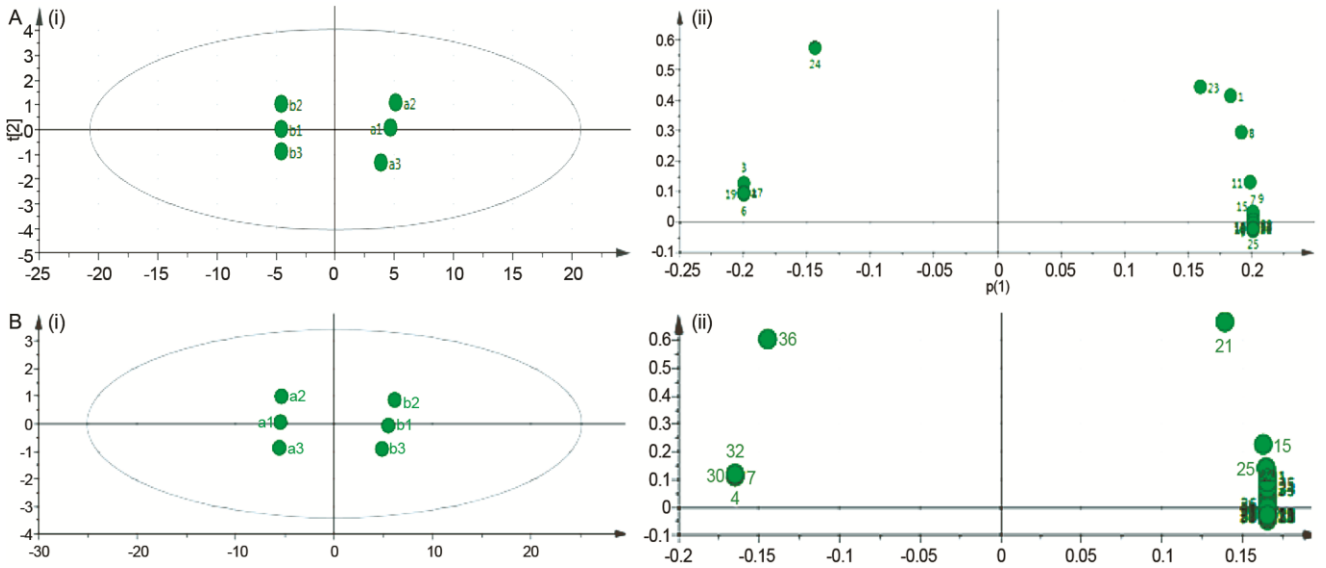

Fig. 3 — PCA analysis between (A) normal control group and model group; and (B) Abietic acid administration group and model group. (i) score chart of samples; and (ii) factor loading diagram

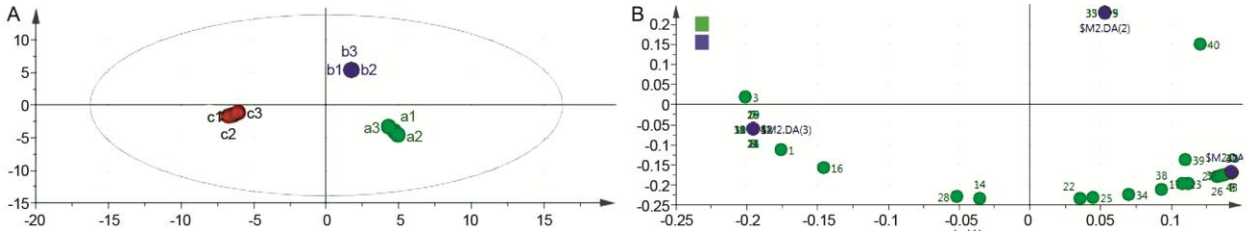

Fig. 4 — PLS-DA analysis between three groups (A) the score chart of samples; and (B) the factor loading diagram

applied to further analyze the differences among the three groups.

Fig. 4 A & B are the sample score chart and molecular (factor) load chart, respectively, which is consistent with the PCA model. Fig. 4A showed that there is significant difference among the three groups. Fig. 4B is the molecular load diagram, which showed that P28, P25, P9, P34 and P5 make a greater contribution to distinguish the three groups.

However, quantitative results cannot be obtained only from the score graph and load graph, so variable importance in projection (VIP) column graph is used to find differential metabolites. Experience indicates that for higher value of VIP, the grouping effect may be greater. Generally, the variable is used as a potential biomarker when VIP >1. The metabolites are analyzed by mathematical statistics, which showed significant difference in the two groups. The metabolite biomarkers were identified as ceramides (Cer), sphingosines, adenosine, 2'-deoxycytidine-5'-monophosphate (dCMP) and lysophosphatidyl-cholines (LPC), and the difference between groups was significantly. Compared with the model group, the contents of ceramides and sphingosines in serum increased significantly in the normal and AA administration groups (P <0.01), but adenine nucleoside, dCMP and lysophosphatidylcholines were decreased obviously (P <0.01). Relevant information of variables with high VIP values was listed in Table 1.

Discussion

Prolonged UVC-irradiations could induce skin injury of BALB/c mice depilated in back. HPLC/QTOF-MS metabolomic analysis of UVC-induced skin injury and effects of AA was investigated to identify differential metabolite markers so as to infer the possible underlying mechanism. The results in this experiment show that UVC radiation can induce seriously pathologic damage to skins. After 8 weeks, the model mice skin tissue showed decrease of irradiated skin elasticity, thickness of cuticle, papillary hyperplasia and ulceration. In UVC radiation model group, the contents of ceramides, sphingosines, glycyl-L-

glutamine and *dihydroorotic acid* were decreased obviously, but adenine nucleoside, dCMP and lysophosphatidylcholines were increased significantly. AA could effectively prevent morphological and pathological changes of UV-irradiation induced photo damage. AA could raise the level of ceramides and sphingosines, and also put adenosine, dCMP and lysophosphatidylcholines down in model mice skin tissue.

Ceramides in skin belong to sphingolipids, which are a class of chemical compounds in which sphingosine and fatty acid are linked by amide linkage. De novo synthesis of ceramides is conducted on endoplasmic reticulum. First, serine and palmitoyl-CoA condense to form 3-ketosphingonine (3-KDS) under catalysis of serine palmitoyl transferase (SP) which is the rate-limiting enzyme. KDS produce sphingosines, and then form ceramides by N-terminal acylation. Other enzymes play the leading role in the process of ceramides metabolism, such as sphingomyelin synthase (SMS), neutral ceramide enzyme (CDcase) and ceramide kinase (CK)[14]. AA might activate the key enzyme SP or inhibit the enzyme in catabolism. Ceramides make up more than half of total stratum corneum lipids. Ceramides participate in the formation of epidermal barrier function, and play major roles in signal transduction, cell proliferation and differentiation, and immune regulation. Abnormal ceramide metabolism may cause skin barrier dysfunction[15]. Skin problems can also interfere with ceramide metabolic pathways, which will affect ceramide content of cuticle. Adenine nucleoside that functions as a good soothing and skin-restoring agent is a constituent of RNA and DNA. The changes of adenosine and dCMP concentration may indicate the nucleic acid damage of skin tissue after UVC radiation exposure. Numerous studies have shown that large amounts of UV radiation can disturb nucleotide metabolism in skin cells and even lead to skin cancer[16]. Intracutaneous injection of lysophosphatidylcholine induces skin inflammation[17]. Ceramides, sphingosines, glycyl-L-glutamine, *dihydroorotic acid*, adenine nucleoside, dCMP and lysophosphatidylcholines are involved in many important metabolic pathways, including sphingolipid metabolism, purine and pyrimidine metabolism, phospholipid metabolism and glutamine metabolism, which play roles in several pathology processes of skin disease such as barrier damage, DNA injury, inflammation and photoaging.

Conclusion

Ceramides, sphingosines, glycyl-L-glutamine, *dihydroorotic acid*, adenine nucleoside, dCMP and lysophosphatidylcholines can be used as biomarkers of UV-induced skin injury. AA can interfere with skin sphingolipid metabolism, purine and pyrimidine metabolism, and the concrete mechanism need further study.

Conflict of Interest

Authors declare no competing interests.

References

1 Simbirtsev AS, Konusova VG, Mchelidze GS, Fidarov EZ, Paramonov BA & Chebotarev VY, Pine resin and biopin ointment: effects on repair processes in tissues. *Bull Exp Biol Med*, 133 (2002), 457.

2 Wiyono B, Tachibana S & Tinambunan D, Chemical Compositions of Pine Resin, Rosin and Turpentine Oil from West Java. *Bull Korean Chem Soc*, 34 (2006) 103. DOI: 10.20886/ijfr.2006.3.1.7-17.

3 Yang NY, Liu L, Tao WW, Duan JA & Tian LJ, Diterpenoids from Pinus massoniana resin and their cytotoxicity against A431and A549 cells. *Phytochemistry*, 71 (2010) 1528. DOI: 10.1016/j.phytochem.2010.06.008.

4 Tian, Lijuan & Yang, Preventive Effect of Abietic Acid against Skin Cancer of Mice. *Nat Prod Comm*, 12 (2017) 1393.

5 Tanaka R, Tokuda H & Ezaki Y, Cancer chemopreventive activity of "rosin" constituents of Pinus spez. and their derivatives in two-stage mouse skin carcinogenesis test. *Phytomedicine*, 15 (2008) 985.

6 Hsieh YS, Yang SF, Hsieh YH, Hung CH, Chu SC, Yang SH & Chen PN, The Inhibitory Effect of Abietic Acid on Melanoma Cancer Metastasis and Invasiveness ***in vitro*** and *in vivo*. *Am J Chin Med*, 43 (2015) 1697. doi.org/ 10.1142/S0192415X15500962.

7 Jeon Y, Jung Y, Youm JK, Kim KH, Cho KH & Eun HC, Abietic acid inhibits UVB-induced MMP-1 expression in human dermal fibroblast cells through PPARα/γ dual activation. *Exp Dermatol*, 24 (2015) 140. doi: 10.1194/jlr.m500105-jlr200.

8 Ichihashi M, Ueda M, Budiyanto A, Bito T, Oka M, Fukunaga M, Tsuru K & Horikawa T, UV-induced skin damage. *Toxicology*, 189 (2003) 21. doi.org/10.1016/S0300-483X(03)00150-1.

9 Kappes UP, Luo D, Potter M, Schulmeister Karl & Rünger TM, Short- and Long-Wave UV Light (UVB and UVA) Induce Similar Mutations in Human Skin Cells. *J Invest Dermatol*, 126 (2006) 667. doi.org/10.1038/ sj.jid.5700093.

10 Herrling T, Jung K & Fuchs J, Measurements of UV-generated free radicals/reactive oxygen species (ROS) in skin. *Spectrochim Acta A: Mol Biomol Spectrosc*, 63 (2006) 840. doi.org/10.1016/j.saa.2005.10.013.

11 Berkey C, Biniek K & Dauskardt RH, Screening Sunscreens: Protecting the Biomechanical Barrier Function of Skin from Solar Ultraviolet Radiation Damage. *Int J Cosmetic Sci*, 39 (2016) 269. doi.org/10.1111/ ics.12370.

12 Abdellah T, Carlos F & Soumeya B, Advances in metabolome information retrieval: turning chemistry into biology. Part I: analytical chemistry of the metabolome. *J Inherit Metab Dis*, 41 (2018) 379. doi.org/10.1007/s10545-017-0074-y.

13 Zhuo ZZ, Liu L, Zhao X, Ma WJ, Zhao Q, Wang YZ & Zhang GY, The effects of UVA and UVB on serum lipid content and antioxydation of ovariectomized rats. *J Toxicol*, 28 (2014) 282.

14 Li Q, Fang H, Dang E & Wang G, The role of ceramides in skin homeostasis and inflammatory skin diseases. *J Dermatol Sci*, 97 (2020) 2.

15 Arct J, Majewski S & Karolina LK, Biological activity of ceramides and other sphingolipids. *Postepy Dermatol Alergol*, 29 (2012) 169. DOI: 10.1159/000339899.

16 Cadet J, André Grand & Douki T, Solar UV Radiation-Induced DNA Bipyrimidine Photoproducts: Formation and Mechanistic Insights. *Topics Curr Chem*, 356 (2014) 249. DOI: 10.1007/128_2014_553.

17 Ryborg AK, deleuran B, Ségaard H & Kragballe K, Intracutaneous Injection of Lysophosphatidylcholine Induces Skin In¯ammation and Accumulation of Leukocytes. *Acta Derm Venereol*, 80 (2000) 242. doi: 10.1080/000155500750012090.